Available online at www.sciencedirect.com
ScienceDirect
Trans. Nonferrous Met. Soc. China 20(2010) 831−838
Transactions of Nonferrous Metals Society of China
www.tnmsc.cn

Effect of ball milling time on microstructures and mechanical properties of mechanically-alloyed iron-based materials

LIU Dong-hua(刘东华), LIU Yong(刘 咏), ZHAO Da-peng(赵大鹏), WANG Yan(王 岩), FANG Jing-hua(方京华), WEN Yu-ren(温玉仁), LIU Zu-ming(刘祖铭)

State Key Laboratory of Powder Metallurgy, Central South University, Changsha 410083, China

Received 9 October 2009; accepted 18 December 2009

Abstract: The microstructures and mechanical properties of an iron-based alloy (Fe-13Cr-3W-0.4Ti-0.25Y-0.30O) prepared by mechanical alloying were investigated with scanning electron microscope, optical microscope, X-ray diffractometer and hardness tester. The results show that the particle size does not decrease with milling time because serious welding occurs at 144 h. The density of the alloy sintered at 1 523 K is affected by the particle size of the powder. Finer particles lead to a high sintered density, while the bulk density by using particles milled for 144 h is as low as 70%. In the microstructures of the annealed alloy, large elongated particles and fine equiaxed grains can be detected. The elongated particle zone has a higher microhardness than the equiaxed grain area in the annealed alloys due to the larger residual strain and higher density of the precipitated phase.
Key words: iron-based alloy powder; mechanical alloying; microstructure; elongated particles; equiaxed grain; residual strain

1 Introduction

Oxide-dispersion strengthened (ODS) nickel- and iron-base superalloys have a wide application in high temperature components[1−3]. ODS steel is a promising material that has the potential to keep microstructural stability and satisfactory mechanical properties even under the high-dose neutron irradiation in fusion reactor as well as fast reactor[4]. ODS ferritic steels are usually prepared via mechanical alloying (MA) of rapidly solidified prealloyed powder Fe-12Cr-3W-0.4Ti and fine ceramic particles (Y_2O_3), and consolidated by densification methods such as hot extrusion, rolling or hot isostatic pressing(HIP)[5−7]. Grain size in the microscale range (1−20 μm) can be obtained due to the high energy milling process[8]. However, a small grain size is associated with low strength and superplastic behavior at elevated temperatures; therefore, nanoscale or ultrafine oxide particles are usually introduced, and their effect on the microstructures and mechanical properties have been extensively investigated[9−10].

The ceramic particles, which decompose or dissolve in the alloy matrix during mechanical alloying, will precipitate as fine or nanostructured particles during subsequent annealing[11]. However, the dissolution of Y_2O_3 is difficult, and needs a long time of milling. Insufficient dissolution of yttrium oxide will lead to an inhomogeneous microstructure even after HIP[12−13].

In this work, a master alloy powder containing Y was oxidized at first and then mechanically alloyed to dissolve the oxygen. The microstructures and mechanical properties were studied by considering the evolution of oxygen and microstructure in the material preparation process.

2 Experimental

The composition of the atomized powders used in this investigation is shown in Table 1. High-purity (>99%) Fe, Cr and W were used as raw materials, while Ti and Y were added in the form of Fe-Ti and Fe-Y alloys. The master alloy was remelted at 1 923 K, and then the melt was atomized in Ar (99.99%) at a pressure of 3−3.5 MPa. The prealloyed powder was oxidized for 4 h at 773 K in the air[14], and the measured average oxygen content was 0.30% (mass fraction). In the MA process, a XQM-2L high-energy planetary ball mill with

Foundation item: Project(50634060) supported by the National Natural Science Foundation of China; Project(50721003) supported by the Creative Research Group of National Natural Science Foundation of China
Corresponding author: LIU Yong; Tel: +86-731-88830406; E-mail: yonliu@mail.csu.edu.cn
DOI: 10.1016/S1003-6326(09)60222-3

four stainless steel pots was used, and each pot contained stainless steel balls in diameters of 10 mm and 6 mm, respectively. The ball-to-powder mass ratio (BPR) was 8:1. The rotation speed was 225 r/min, and the milling time of 100, 144 and 200 h was adopted, respectively. Powder handling and sampling were performed in a glove box under high purity Ar atmosphere.

Table 1 Compositions of iron-based atomized powder (Mass fraction, %)

Cr	W	Ti	Y	O	Fe
13.15	3.30	0.43	0.25	0.033	Bal.

The raw bars were fabricated by sintering the MA powder at 1 523 K, hot forging at 1 473 K, and finally annealing at 1 123 K for 1 h. Density was measured geometrically in a Quantachrome Multipycnometer using helium displacement gas for as-sintered samples. Powder particle size distribution was determined by using Malven microplus laser scatter tester. For more detailed study on the microstructures, an FEI Tecnai G^2 20 transmission electron microscopy (TEM) was used, operated at 200 kV.

The metallographic examinations were carried out using a MeF3A optical microscope. The phase constitutions of the milling powder were determined by using a Rigaku D/max 2550VB$^+$ X-ray diffractometer (XRD), with a Cu K_α target, scanning at a voltage of 40 kV, a current of 200 mA and a speed of 8 (°)/min. The observation of the morphology of powder was conducted on a JSM-6360 LV scanning electron microscope (SEM). The chemical compositions in the particles and alloys were semi-quantitatively determined by using energy diffraction spectroscopy (EDS). Vickers microhardness tests for the annealed alloys were performed by using HVS-1000 at a load of 0.245 N.

3 Results

3.1 Characteristics of powder

Fig.1 shows the cross-sectional morphology and the chemical composition of oxidized iron-based powder. It can be seen that, although the oxygen content at the edge of the particles is clearly higher than that inside the particles, the oxidized layer could not be observed on the surface of the particles. This implies that the reaction between iron-based powder and oxygen is very slow.

The solubility of O in Fe matrix is only 0.03% (mass fraction) in equilibrium. However, the O content in the Fe matrix is as high as 0.11%, significantly higher than expected. Therefore, most oxygen should be in the form of oxide on the surface of the particles.

Fig.2 shows the cross-sectional morphology and chemical composition of MA powder. It may be noted that oxygen content inside particles is similar with that at the edge of particles, indicating a homogenous distribution of O in the whole particle by MA.

Fig.3 shows the change of the particle size with the milling time as well as the corresponding microstructures. After ball milling, the particles firstly change from spherical to irregular shape with rough surfaces, and then become granular in shape with increasing milling time. The particle size decreases with increasing milling time. It is found that the particles re-weld obviously at the milling time of 144 h, and are large in size. After milling for 200 h, the particle size of the oxidized atomized powder is about 2 μm.

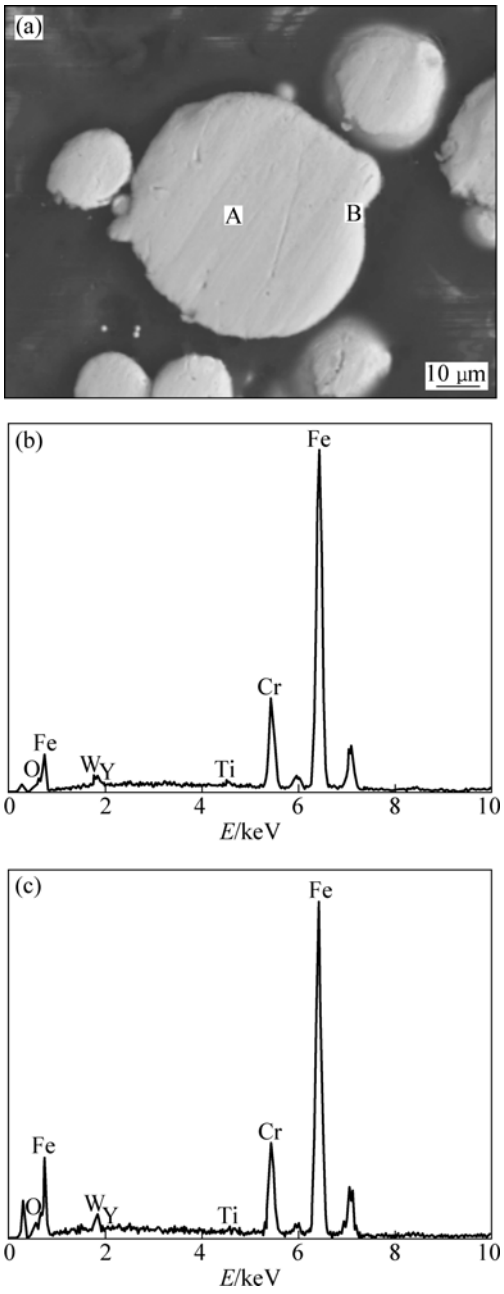

Fig.1 Cross-sectional morphology of oxidized iron-based powder particles (a) and chemical analysis results of Position A (b) and Position B (c) marked in (a), respectively

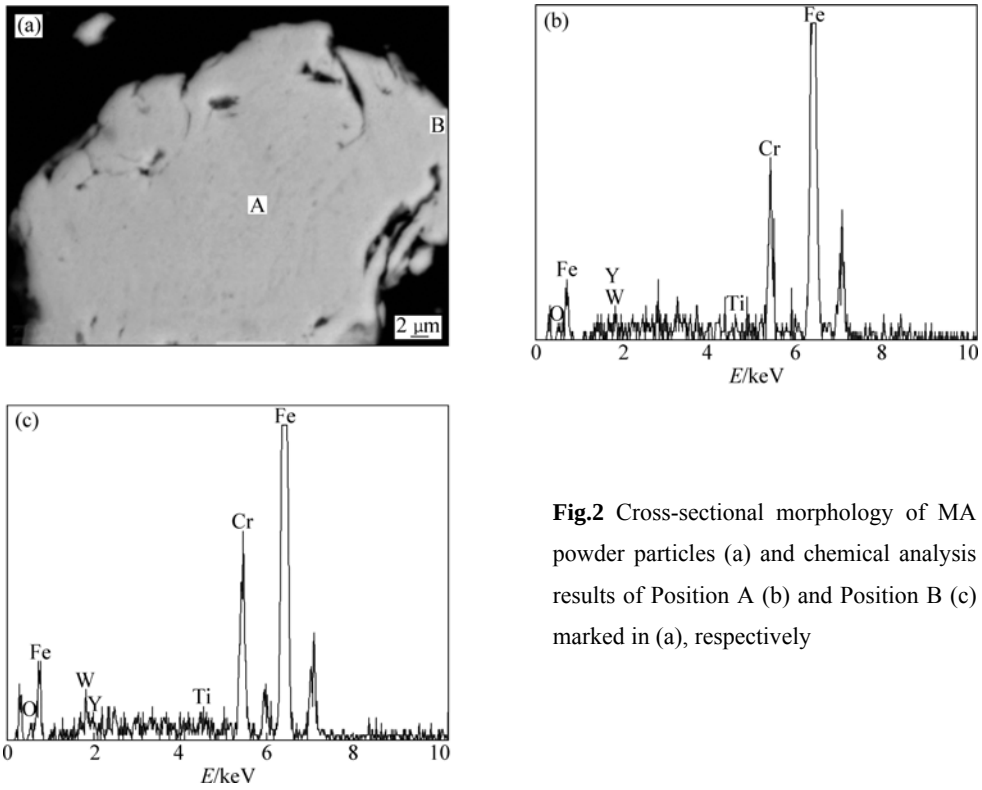

Fig.2 Cross-sectional morphology of MA powder particles (a) and chemical analysis results of Position A (b) and Position B (c) marked in (a), respectively

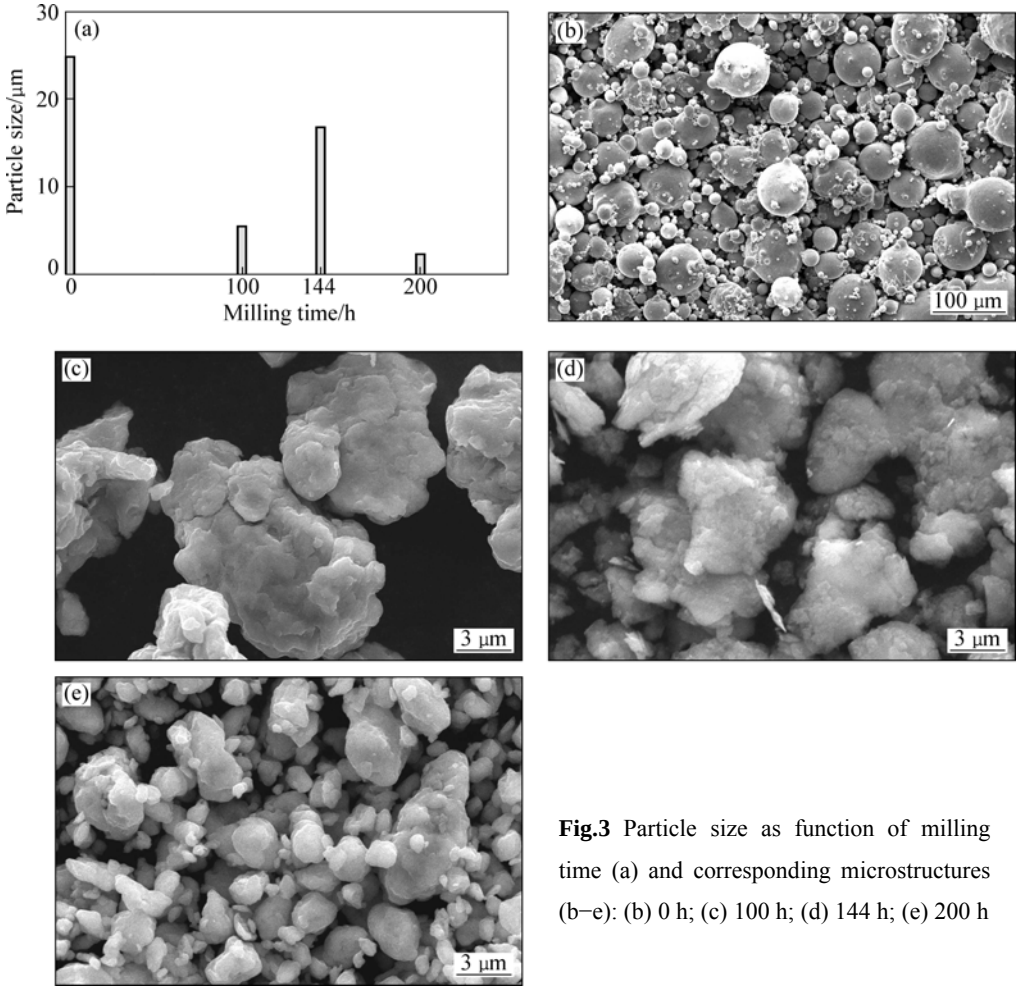

Fig.3 Particle size as function of milling time (a) and corresponding microstructures (b−e): (b) 0 h; (c) 100 h; (d) 144 h; (e) 200 h

3.2 Phase composition of mechanically alloyed powder

Fig.4 shows the X-ray diffraction patterns of the mechanically alloyed powder for different milling time. It is shown that the alloy is mainly composed of the Fe-Cr phase, which does not change much during the whole MA process. The XRD peaks become broader with increasing milling time. With the milling time increasing to 200 h, the peak of Fe (220) becomes weaker obviously.

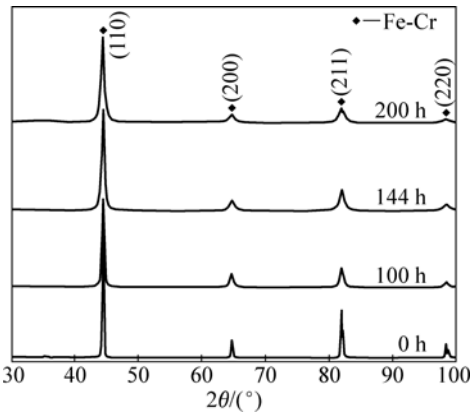

Fig.4 XRD patterns of powders milled for different time

The peak broadening detected in the patterns suggests that both the grain size of the mixed powders and the change in lattice distortion are significantly affected by the mechanical milling. The structurally broadened profile is given by[15]

$$\beta^2 = [K\lambda/(D\cos\theta)]^2 + (4e\cdot\tan\theta)^2 \quad (1)$$

where K is the Scherrer factor, ≈1; θ is the Bragg angle; λ is the X-ray wavelength; and β is the full width at half maximum (FWHM). Plotting $\beta^2\cos^2\theta/\lambda^2$ against $\sin^2\theta/\lambda^2$ for the two orders of reflection ({110} and {220} in this work) and extrapolating the line to $\sin^2\theta/\lambda^2=0$ allows the estimation of $1/D^2$ and the slope of the line yields $16e^2$, from which the grain size D and microstrain e are calculated. Table 2 shows the grain size and the microstrain of the milled powders for different milling time. Before mechanical alloying, the particle size is 24.88 μm as shown in Fig.3, without microstrain. After mechanical alloying, all the peaks in the XRD pattern for the Fe-Cr phase are broadened. The grain size of structure is in the range from 18.5 to 55.2 nm. The grain size of the powder milled for 200 h is 18.5 nm, which confirms the TEM observation of grain size (10−30 nm). The calculated values of the grain size and the microstrain for the powder milled for 144 h are 40.3 nm and 0.28%, respectively.

3.3 Microstructure evolution

The microstructures of the as-sintered alloys are shown in Fig.5. It can be seen that the microstructure consists of coarse primary particles and fine grains. The microstructure of the coarse particles consists of several grains. As for the powder milled for 200 h, the grain size of the sintered alloy is very fine and only a few coarse primary particles distribute in the matrix.

Table 2 Grain size and microstrain after different milling time

Ball milling/h	Grain size/nm	Microstrain/%
100	55.2	0.14
144	40.3	0.28
200	18.5	0.09

The relative densities of the compacts and the as-sintered alloys are shown in Table 3. The relative densities of the compacts by using the mechanically alloyed powders show similar results. However, the alloys made by fine particles milled for 100 h and 200 h have a higher relative density than alloys made by coarse particles milled for 144 h.

The microstructures of the annealed alloys are shown in Fig.6, where the horizontal direction

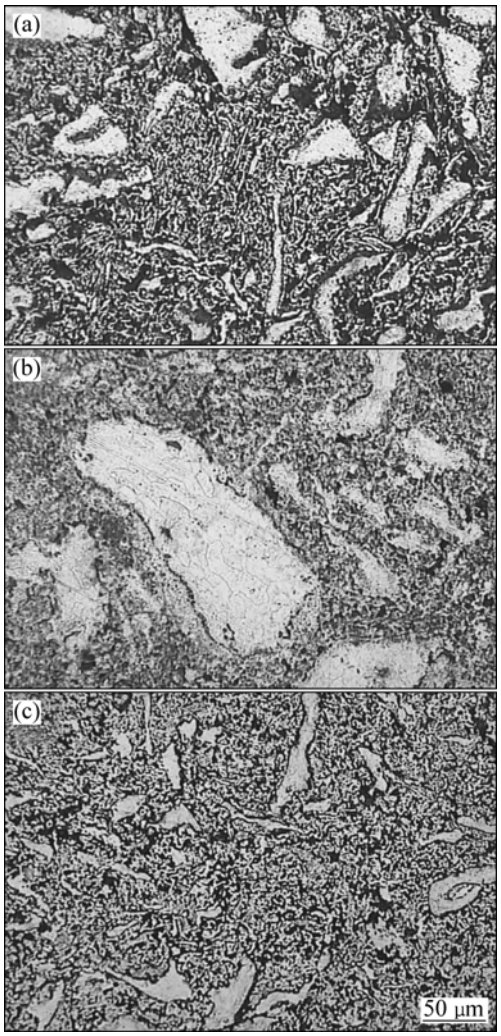

Fig.5 Microstructures of sintered alloys by using powders milled for 100 h (a), 144 h (b) and 200 h (c)

corresponds to the direction of hot-forging. With large deformation, the alloys have a microstructure consisting of the elongated particles and equiaxed grains. The original large particles exhibit preferred orientation along the forging direction. It shows the similar microstructures with 9Cr-ODS martensitic steels[16] using high energy ball milling with elemental powders, and hot-extrusion. The elongated particles in the specimen made by powder milled for 144 h are larger than those in other specimens.

Table 3 Relative density of compacts and as-sintered alloys with powders milled for different time

Material	Milling time/h		
	100	144	200
Compact	60.1%	61.2%	58.8%
As-sintered alloy	87.7%	70.4%	88.1%

The EDS results of the particle boundary, the elongated particles and the equiaxed grains are shown in Fig.7. It can be seen that the contents of Cr and oxygen

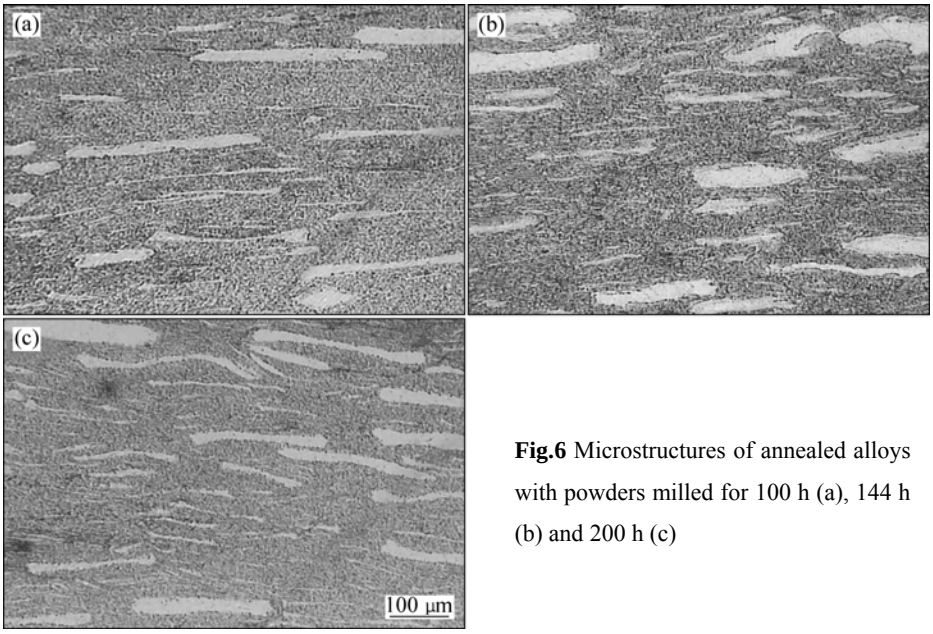

Fig.6 Microstructures of annealed alloys with powders milled for 100 h (a), 144 h (b) and 200 h (c)

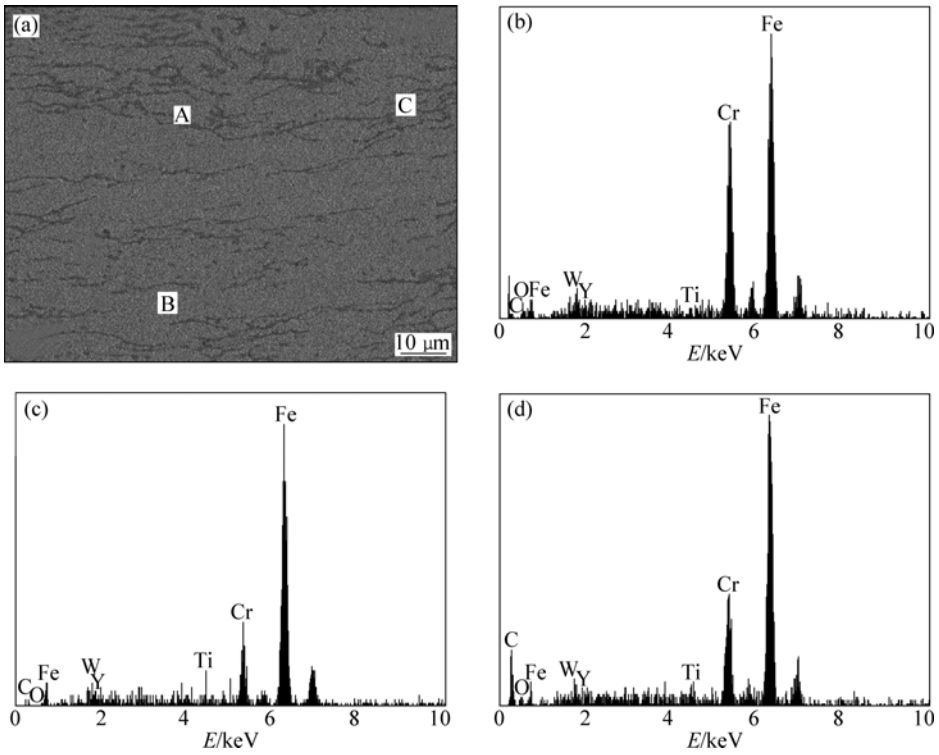

Fig.7 Backscattered electron image of annealed alloy (a), and EDS results of grain boundary A (b), elongated particle B (c) and equiaxed grain C (d) marked in (a), respectively

in the elongated particles and the equiaxed grain are lower than those at the grain boundary. The contents of Ti, Y and oxygen in the equiaxed grain are higher than those in the elongated particles.

TEM observations of powder milled for 200 h and the annealed alloy are shown in Fig.8. The grain size is estimated to be 15−30 nm, which confirms the XRD calculation of grain size (18.5 nm). No presence of the precipitates is found, which has been confirmed by MILLER et al[17]. The oxygen has completely been dissolved. The precipitated phase are formed in both the coarse primary particles and the fine grains(Fig.8(b)). The precipitated phases in the elongated particles are more than those in the equiaxed grains.

3.4 Vickers microhardness

Vickers microhardness of the annealed alloys made by powders of different milling time is shown in Fig.9. It is interesting to note that the microhardness in the elongated particles is much higher than that in the equiaxed grains. Vickers microhardness of the equiaxed grains increases with the increasing milling time. However, the maximum microhardness of the elongated particles appears at the milling time of 144 h.

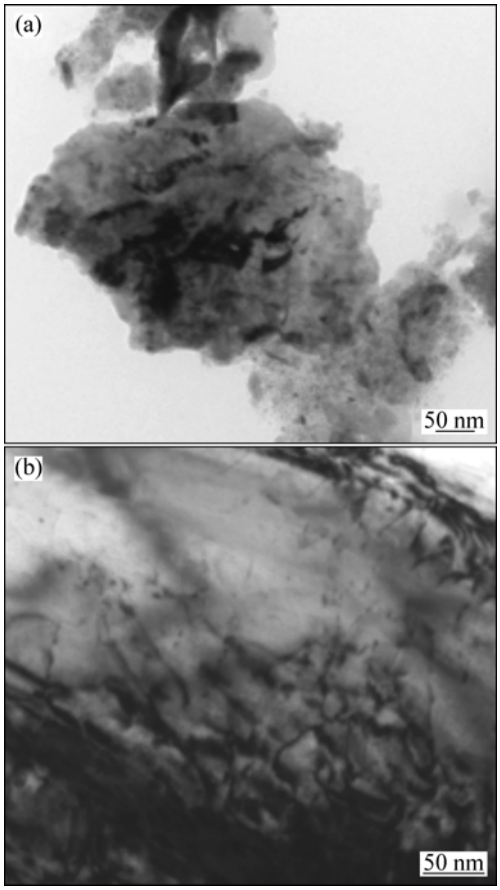

Fig.8 TEM bright field images of as-milled powder at 200 h (a) and annealed alloy (b)

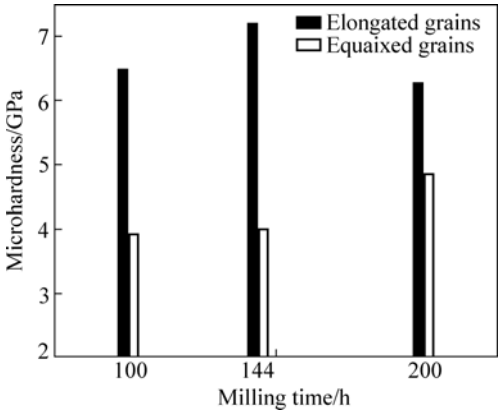

Fig.9 Vickers microhardness of annealed alloys

4 Discussion

4.1 Evolution mechanism of powder particles during MA process

Mechanical alloying is a solid-state powder processing involving repeated welding, fracturing, and re-welding of particles in a high-energy ball mill. The oxide film of the oxidized powders can be fractured and the oxygen can be dissolved into the powders during mechanical alloying, as shown in Fig.2. The XRD result also indicates the single-phase state of the powder (Fig.4). The grain size of the MA powder decreases with increasing milling time. Fine particle sizes ranging 1−5 μm for the atomized powder after MA are formed at the milling time of 100 h and 200 h (Fig.3). However, the agglomerated particles are obviously observed at the milling time of 144 h, with the particle size of 16.7 μm (Fig.3). Therefore, serious welding occurred at this time interval.

Mechanical alloying process and the serious welding of iron-based alloy powders can be explained by the model proposed by MAURICE and COURTNEY[18]. First, the powder particles with good flowability and low friction can be deformed by the collision force of the impact, plastically leading to work hardening and fracture. With continued deformation, the particles get work-hardened and fracture by a fatigue failure mechanism and by the fragmentation of fragile flakes. Fragments generated may continue to reduce their size due to the absence of strong agglomerating forces (Fig.3(b)). Second, the surface energy of the particles increases with the new surfaces of particles increasing. The self-binding can occur among the fractured particles, which is caused by the interaction among particles. The interaction is also named as the van der Waals force. The powder particles with poor flowability, irregular surfaces and high friction are sandwiched between two steel balls. Therefore, the self-binding enables the particles to weld together, leading to an increase in the particle size. The

tendency of welding together and forming large particles at the milling time of 144 h is strong, as seen from Fig.3(c). In this stage, the tendency to agglomerate particles is high. Third, after milling for a certain time, the steady-state equilibrium is attained when a balance is achieved between the rate of welding, which can increase the average particle size, and the rate of fracturing, which tends to decrease the average particle size. The range of the particle size distribution in this stage is narrow and the average particle size is small (Fig.3(d)).

4.2 Microhardness

OHTSUKA et al[16] demonstrated that the microhardness in the matrix consisting of the elongated grains and the equiaxed grains is less than 3.5 GPa. Our recent work shows that the fine (10−20 nm) Y-Ti-rich oxides are found in the ferritic steels using atomization powder without MA; and the microhardness of the ferritic steel is as high as HV 6.1 GPa. However, the microhardness of the iron-based steel in this work is 4.0−7.1 GPa. The reason may be that the MAed powder alloy has the finer grain size and the precipitates of Cr. During the MA process, Cr is distributed uniformly in the fine and coarse particles. The content of Cr in the equiaxed grains may increase after annealing, due to the grain boundary and interface segregation of Cr (Fig.7). A pronounced Cr segregation to the oxide particle interface was found after annealing at 700 ℃ in a Fe-Cr alloy[19]. The Cr contents in the elongated particles and the equiaxed grains are lower than those at the grain boundary because the large particles have a smaller amount of the interface. The hardness of the alloy steels could be increased with increasing the content of Cr.

The microhardness in the equiaxed grains is much lower than that in the elongated particles. The result is the same as that of UKAI and FUJIWARA[20]. The large particles actually have a large strain during MA, which cannot be recovered in the subsequent annealing. On the other hand, recovering and crystallization may easily occur in the fractured or sandwich-like particles. Therefore, the microhardness in the elongated particles is higher than that in the equiaxed grains. Another factor that may contribute to the different microhardness of the iron-based steel is the non-uniform distribution of precipitated phase. The matrix alloy can be strengthened by the precipitated phase. The reinforcement is affected by the size and the distribution of the particles. The precipitated phases in the elongated particles are more than those in the equiaxed grain, so the elongated particles have a higher strength than the equiaxed grains.

5 Conclusions

1) In the Fe-based powder, the grain size of the MA powder decreases with increasing milling time; however, the particle size does not decrease linearly with milling time. Serious cold-welding occurs at the milling time of 144 h.

2) The relative density of the as-sintered alloys is influenced by the particle size of the powders before sintering. The coarse particles lead to a low density in the sintered alloys.

3) The microhardness in the elongated particles is higher than that in the equiaxed grains, which is caused by the larger residual strain and higher density of the precipitated phase.

References

[1] IAMAIL O, SASCHA A, SILKE M, BERNHARD W. Nanocrystalline Al–Al_2O_{3p} and SiC_p composites produced by high-energy ball milling [J]. Journal of Materials Processing Technology, 2008, 205(1/3): 111−118.

[2] CHEN Bo-qu, YANG Sha, LIU Xing-xing, YAN Biao, LU Wei. A study on nanocrystallization of alloy $Fe_{73}Cu_1Nb_{1.5}V_2Si_{13.5}B_9$ by high-energy ball milling [J]. Journal of Alloys and Compounds, 2008, 448: 234−237.

[3] OLESZAK D, GRABIAS A, PEKALA M, ŚWIDERSKA-ŚRODA A, KULIK T. Evolution of structure in austenitic steel powders during ball milling and subsequent sintering [J]. Journal of Alloys and Compounds, 2007, 434/435: 340−343.

[4] RAMAR A, OKSIUTA Z, BALUC N, SCHAUBLIN R. Effect of mechanical alloying on the mechanical and microstructural properties of ODS EUROFER 97 [J]. Fusion Engineering and Design, 2007, 82: 2543−2549.

[5] UKAI S, NISHIDA T, OKUDA T, YOSHITAKE T. R&D of oxide dispersion strengthened ferritic martensitic steels for FBR [J]. Journal of Nuclear Materials, 1998, 258/263: 1745−1749.

[6] YU G, NITA N, BALUC N. Thermal creep behaviour of the EUROFER 97 RAFM steel and two European ODS EUROFER 97 steels [J]. Fusion Engineering and Design, 2005, 75/79: 1037−1041.

[7] SAKASEGAWA H, OHTSUKA S, UKAI S, TANIGAWA H, FUJIWARA M, OGIWARA H, KOHYAMAD A. Microstructural evolution during creep of 9Cr-ODS steels [J]. Fusion Engineering and Design, 2006, 81: 1013−1018.

[8] MILLER M K, HOELZER D T, KENIK E A, RUSSELL K F. Stability of ferritic MA/ODS alloys at high temperatures [J]. Intermetallics, 2005, 13: 387−392.

[9] CASTRO V D, LEGUEY T, MUNOZ A, MONGE M A, FERNANDEZ P, LANCHA A M, PAREJA R. Mechanical and microstructural behaviour of Y_2O_3 ODS EUROFER 97 [J]. Journal of Nuclear Materials, 2007, 367/370: 196−201.

[10] MILLER M K, FU C L, KRCMAR M, HOELZER D T, LIU C T. Vacancies as a constitutive element for the design of nanocluster-strengthened ferritic steels [J]. Shanghai Metals, 2008, 30(4): 1−6. (in Chinese)

[11] ALINGER M J, ODETTE G R, HOELZER D T. On the role of alloy composition and processing parameters in nanocluster formation and dispersion strengthening in nanostructured ferritic alloys [J]. Acta Materialia, 2009, 57: 392−406.

[12] MILLER M K, RUSSELL K F, HOELZER D T. Characterization of precipitates in MA/ODS ferritic alloys [J]. Journal of Nuclear Materials, 2006, 351(1/3): 261−268.

[13] KLUEH R L, SHINGLEDECKER J P, SWINDERMAN R W, HOELZER D T. Oxide dispersion-strengthened steels: A comparison of some commercial and experimental alloys [J]. Journal of Nuclear Materials, 2005, 341(2/3): 103−114.

[14] LIU Dong-hua, LIU Yong, HUANG Bai-yun, ZHANG Ning-yi, FANG Jing-hua, LIU Feng. High temperature oxidation behavior of iron-based metal powder [J]. The Chinese Journal of Nonferrous Metals, 2008, 18(12): 2166−2171. (in Chinese)

[15] GUO Z, KEONG K G, SHA W. Crystallisation and phase transformation behaviour of electroless nickel phosphorus platings during continuous heating [J]. Journal of Alloys and Compounds, 2003, 358: 112−119.

[16] OHTSUKA S, UKAI S, FUJIWARA M, KAITO T, NARITA T. Improvement of 9Cr-ODS martensitic steel properties by controlling excess oxygen and titanium contents [J]. Journal of Nuclear Materials, 2004, 329/333: 372−376.

[17] MILLER M K, HOELZER D T, KENIK E A, RUSSELL K F. Nanometer scale precipitation in ferritic MA/ODS alloy MA957 [J]. Journal of Nuclear Materials, 2004, 329/333: 338−341.

[18] MAURICE D, COURTNEY T H. Modeling of mechanical alloying: Part I. Deformation, coalescence and fragmentation mechanisms [J]. Metallurgical and Material Transaction, 1994, A25: 147−158.

[19] KRAJNIKOV A V, ORTNER H M, WEINBRUCH S, GROGGER W, WARBICHLER P, HOFER F, YURCHENKO V M. Chromium interaction with TiO_2 dispersoids in oxide dispersion strengthened ferritic steel [J]. Materials Science and Technology, 1999, 15: 1425−1432.

[20] UKAI S, FUJIWARA M. Perspective of ODS alloys application in nuclear environments [J]. Journal of Nuclear Materials, 2002, 307/311: 749−757.

(Edited by YANG Bing)